Available online at www.sciencedirect.com
SCIENCE DIRECT
Journal of Catalysis 231 (2005) 92–104
JOURNAL OF CATALYSIS
www.elsevier.com/locate/jcat

Mechanism of reconstitution of hydrotalcite leading to eggshell-type Ni loading on Mg–Al mixed oxide

Katsuomi Takehira [a,*], Tomonori Kawabata [a], Tetsuya Shishido [b], Kazuhiro Murakami [a], Takenori Ohi [a], Daisuke Shoro [c], Masahide Honda [c], Ken Takaki [a]

[a] *Department of Chemistry and Chemical Engineering, Graduate School of Engineering, Hiroshima University, Kagamiyama 1-4-1, Higashi-Hiroshima 739-8527, Japan*
[b] *Department of Chemistry, Tokyo Gakugei University, Koganei, Tokyo 184 8501, Japan*
[c] *Hiroshima Prefectural Institute of Industrial Science and Technology, Kagamiyama 3-10-32, Higashi-Hiroshima 739-0046, Japan*

Received 7 December 2004; revised 17 January 2005; accepted 21 January 2005

Abstract

The mechanism of eggshell-type Ni loading on Mg–Al mixed oxide particles has been carefully studied in connection with the structure of the mixed oxides as the catalyst supports. The pore distribution, surface morphology, and crystal and coordination structure of the mixed oxides were studied by XRD, MAS-NMR, TG-DTA, SEM, TEM, ICP, and N_2 and H_2 adsorption methods. The Mg–Al mixed oxide was prepared as a powder by calcining Mg–Al hydrotalcite and pressing it into the particles. When the particles were dipped in an aqueous solution of Ni^{2+} nitrate, reconstitution of Mg–Al hydrotalcite took place in the surface layer of the particles, and simultaneously Ni^{2+} replaced a part of the Mg^{2+} sites by a "memory effect" of the hydrotalcite structure. The reconstitution by memory effect took place for periclase Mg(Al)O that formed from Mg–Al hydrotalcite by the calcination at low temperature and at a low rate of heating. The memory effect proceeded by a dissolution–recrystallization mechanism on the microporous phase and formed "worm-like" structures, which finally constituted a dense layer and covered the surface of the particles. The dense layer hindered the further penetration of Ni^{2+} nitrate solution into the cores of the particles, resulting in eggshell-type Ni loading. A balance between the rate of reconstitution of Mg–Al hydrotalcite and the rate of penetration of the aqueous solution of nickel nitrate determined the loading type of Ni. Eggshell-type loaded Ni catalyst showed an enhanced activity per unit amount of Ni due to the surface enrichment of active Ni species, since measurement of the effectiveness factor of the catalyst showed that the intraparticle mass transfer limitation exists in steam reforming of CH_4 over the catalyst at 1073 K.

Keywords: CH_4 reforming; H_2 production; Eggshell-type loaded Ni catalyst; Mg–Al hydrotalcite; Reconstitution; Memory effect; Effectiveness factor

1. Introduction

Hydrogen production for polymer electrolyte fuel cells (PEFCs) is an important research area worldwide. Steam reforming of CH_4 is the largest and generally the most economical way to make H_2 [1–3], and autothermal reforming is under development as an alternative industrial chemical approach. Both processes still require further advancement in the preparation of potent reforming catalysts. The authors have proposed a solid-phase crystallization (*spc*-) method for the preparation of highly dispersed and stable metal-supported catalysts, starting from perovskite materials [4,5] and hydrotalcite-like compounds [6–13] as the precursors. *spc*-Ni/MgAl catalysts were prepared starting from Mg–Al hydrotalcite containing Ni at the Mg sites as the precursors and were successfully applied to partial oxidation [6,7], steam reforming [8,9], and CO_2 reforming of CH_4 [10–12].

In recent years there has been an increased interest in using hydrotalcite-like compounds as precursors for mixed-oxide catalysts in various reactions (as reviewed by Cavani et al. [13]). Indeed, Clause et al. [14] reported that the cat-

* Corresponding author. Fax: (+81-824)-24-7744.
E-mail address: takehira@hiroshima-u.ac.jp (K. Takehira).

0021-9517/$ – see front matter
doi:10.1016/j.jcat.2005.01.025

alysts obtained by thermal decomposition of Ni–Al hydrotalcite precursors have very interesting properties, such as high thermal stability and good metal dispersion. The latter behavior has been attributed by Kruissink et al. [15] to the particular structure of the hydrotalcite through a homogeneous distribution of the metallic cations in the brucite-type sheets. Several attempts to prepare supported Rh and Ni catalysts from Mg–Al hydrotalcite-type precursors for CH_4 reforming have also been reported and claimed in patents by Basile and Vaccari [16–22], Bhattacharyya et al. [23–26], and Hou and Yashima [27]. Both Ni [15–19,21–27] and Rh [17,19–22] catalysts prepared from Mg–Al hydrotalcite precursors showed high and stable activity in partial oxidation [18,19,21,22], steam reforming [23–27], and CO_2 reforming [19,23–27] of CH_4. Shulze et al. [28] reported that the Ni catalysts were also effective for the partial oxidation of light paraffins, such as propane. Recently we reported that *spc*-Ni/MgAl catalyst showed high and stable activity for both steam reforming and autothermal reforming of CH_4. A long catalyst life of 600 h was attained in the former reaction [9], and high CH_4 conversion reaching thermodynamic equilibrium, even at high space velocity (9×10^5 ml h^{-1} g_{cat}^{-1}), was attained in the latter reaction [7], which corresponds to the result obtained with 1 wt% Rh/MgO, which was reported by Ruckenstein and Wang [29] to be the best catalyst.

Hydrotalcite is an anionic clay with layered mixed hydroxides containing exchangeable anions. With heating it yields a mixed oxide with an interesting property, a "memory effect" [13]. This memory effect allows the reconstitution of the original hydrotalcite structure under mild conditions when the product of the thermal treatment is brought into contact with aqueous solutions containing various anions. This memory effect of calcined hydrotalcite is often detrimental to the catalyst activity and lifetime; the reconstitution of hydrotalcite under reaction conditions deactivates the Mg–Al-based catalysts in mercaptan oxidation reactions by inducing the segregation of single-oxide phases, leading to the formation of inhomogeneous, low-surface-area mixed oxides [30,31]. In contrast, when heat-treated hydrotalcites are brought into contact with water at room temperature, reconstitution of the layered structure with mainly OH^- ions in the interlayer proceeds, yielding a highly active base catalyst suitable for liquid-phase aldol condensation reactions [32–35].

We have reported the preparation of eggshell-type loaded Ni catalyst with the use of the memory effect on the surface of oxide particle after thermal treatment [36]; Mg–Al hydrotalcite was reconstituted on the surface of the particles, and some of the Mg^{2+} sites were replaced with Ni^{2+}, resulting in the formation of eggshell-type Ni loaded catalyst, referred to as *s(surface)-spc*-Ni/MgAl. The formation of eggshell-type Ni loading was substantially affected by the conditions of preparation of Mg–Al mixed oxide [37]. In the present paper, we focus on critical phenomena of the memory effect depending on the conditions of calcination treatment of Mg–Al hydrotalcite and clarify the mechanism of eggshell-type Ni loading and its effectiveness in steam reforming.

2. Experimental

2.1. Catalyst preparation

We prepared eggshell-type Ni loaded catalysts (*s-spc*-Ni/MgAl catalysts) by dipping particles of Mg–Al(3/1) mixed oxides in an aqueous solution of Ni^{2+} nitrate, followed by calcination. Mg–Al(3/1) hydrotalcite, $[Mg_6Al_2(OH)_{16}CO_3] \cdot 4H_2O$, was prepared by co-precipitation of nitrates of each metal component [36–38]. An aqueous solution containing the nitrates of Mg^{2+} and Al^{3+} was added slowly with vigorous stirring to an aqueous solution of sodium carbonate. When the pH of the solution was adjusted to 10 with an aqueous solution of sodium hydroxide, a heavy slurry precipitated. After the solution was aged at 363 K for 12 h, the precipitate, $[Mg_6Al_2(OH)_{16}CO_3] \cdot 4H_2O$, was washed with de-ionized water, dried in air at 378 K, and calcined in a muffle furnace in a static air atmosphere under various conditions (with a changing rate of heating and calcination temperature; Table 1). We calcined several samples with changing heating rates of 0.83, 1.67, and 3.33 K min^{-1} to 1123 K, and others were calcined at 823, 923, 1023, 1123, and 1223 K at a fixed heating rate of 1.67 K min^{-1}. All samples were kept for 5 h at the final calcination temperature. The Mg–Al(3/1) mixed oxides, thus obtained, were pressed at 25 tons, crushed and sieved into particles 0.36–0.60 mm⌀ in diameter, and used as a support for the preparation of eggshell-type loaded Ni catalysts. The Mg–Al(3/1) mixed-oxide particles as the supports were dipped in an aqueous

Table 1
Surface area and pore volume of Mg–Al(3/1) mixed oxide[a]

	Surface area (m^2 g_{cat}^{-1})	Pore volume (ml g_{cat}^{-1})
Mg–Al(3/1)-hydrotalcite	117.2	0.372
Heating rate[b] (K min^{-1})		
0.83	146.5	0.367
1.67	110.4	0.287
3.33	88.8	0.257
Calcination temperature[c] (K)		
823	130.7	0.328
923	164.8	0.404
1023	108.8	0.263
1123	110.4	0.287
1223	100.9	0.307
After dipping[d]	0.0	0.006

[a] Mg–Al(3/1) hydrotalcite was prepared by co-precipitation, heated from room temperature to a described temperature at a described rate and calcined at a described temperature for 5 h.
[b] Calcined at 1123 K.
[c] Heated at a rate of 1.67 K min^{-1}.
[d] Heated at a rate of 1.67 K min^{-1} to 923 K, followed by dipping in 1.0 M Ni^{2+} nitrate aqueous solution at pH = 4.7 for 30 min and drying at 378 K.

solution of 1.0 M Ni^{2+} nitrate at pH 4.7 for varying times of 15 to 60 min at ambient temperature. The particles were washed with de-ionized water, dried at 378 K, and calcined at 1123 K for 5 h to form the eggshell-type loaded Ni/MgAl catalysts.

As a control, *spc*-Ni/MgAl and *imp*-Ni/MgAl catalysts were prepared as reported previously [7,9]. The former was prepared by co-precipitation of the nitrates of each metal component, followed by drying and calcination. The latter was prepared by the incipient wetness method: the Mg–Al(3/1) mixed oxide particles were dipped in aqueous or acetone solution of Ni^{2+} nitrate, followed by drying and calcination. These are referred to as *imp*-Ni/Mg_3Al-aq and *imp*-Ni/Mg_3Al-ac, respectively.

The samples for MAS ^{27}Al NMR measurements were prepared by calcination of Mg–Al hydrotalcite at the prescribed temperature and kept for 5 h. The rate of heating was fixed at 1.67 K min^{-1}. We carried out Ni loading by dipping Mg–Al mixed oxide in 0.1 N Ni^{2+} nitrate aqueous solution. The loading amount was as low as 1.3 wt% after the calcination, since Ni^{2+} is paramagnetic and the high-concentration loading did not result in the appearance of a signal in the MAS ^{27}Al NMR spectrum.

2.2. Characterization of catalyst

The structure of the catalysts was studied by XRD, MAS-NMR, TG-DTA, SEM, TEM, ICP, and N_2 and H_2 adsorption methods. Powder X-ray diffraction was recorded on a Rigaku powder diffraction unit (RINT 2250VHF) with monochromatized Cu-K_α radiation ($\lambda = 0.154$ nm) at 40 kV and 300 mA. The diffraction pattern was identified by a comparison with those included in the data base of the Joint Committee of Powder Diffraction Standards (JCPDS). A magic-angle spinning (MAS) ^{27}Al nuclear magnetic resonance (NMR) spectrum was obtained with a Bruker AMX 400 spectrometer at a magnetic field of 9.4 T. The spectrum was recorded at a resonance frequency of 104.26 MHz and a rotor-spinning rate of 3 kHz. The pulse length was 1.0 μs, and 4096 scans were accumulated for each spectrum. Chemical shifts were given relative to a 1 M aqueous aluminum nitrate solution. The molar ratio of octahedrally coordinated Al^{3+} cations (Al_{Oh}) to tetrahedrally coordinated Al^{3+} cations (Al_{Td}) was calculated with γ-Al_2O_3 as a standard reference. TG-DTA was recorded under an inert atmosphere of N_2 (20 ml min^{-1}) with Shimadzu TGA-50 and DTA-50 analyzers, with 50 mg of sample, at a rate of 10 K min^{-1}. A scanning electron micrograph (SEM) was obtained with a JEOL JSM-6340F instrument equipped with a Link SATW EDS. The particles were fixed after drying at 378 K on a sample holder with epoxy resin and polished, and a cross section of the particle was measured by SEM-EDS. A transmission electron micrograph (TEM) was obtained with a JEOL JEM3000F instrument equipped with a Hitachi/Kevex H-8100/Delta IV EDS. The number of Ni metal particles counted in the TEM image to evaluate the distribution was fixed at 200 in each sample. ICP measurement was carried out with a Perkin–Elmer OPTIMA 3000. The content of the metal component was determined after the sample was completely dissolved with diluted hydrochloric acid and a small amount of hydrofluoric acid. N_2 adsorption (77 K) was used to examine both the BET surface area and the porous property of the Mg–Al mixed oxide. The measurement was carried out on a Bell Japan Belsorp 18SP device (volumetric), and all samples were pretreated in vacuum at 473 K for 12 h before the measurements. The pore size distribution was evaluated from the adsorption isotherm by the Dollimore and Heal (DH) method [39]. Ni dispersion was determined by static equilibrium adsorption of H_2 at ambient temperature with the pulse method. Twenty milligrams of the catalyst was reduced at 1173 K in a mixed gas flow of 20 vol% H_2/N_2 (25 ml min^{-1}) for 1 h and used for the measurement. During the pulse experiment, the amount of H_2 was monitored with a TCD-gas chromatograph. Uptake of H_2 at monolayer coverage of the Ni species was used to estimate Ni metal dispersion and particle size.

2.3. Catalytic testing

Steam reforming of CH_4 was conducted with a fixed-bed flow reactor in a mixed gas flow of CH_4 and H_2O (1/2 v/v) at 1073 K over 50 mg of the catalyst for 50 h. The catalyst was used as particles with an average size of 0.48 mm∅ (0.36–0.60) dispersed in quartz sand. N_2 gas was added as an internal standard. A U-shaped quartz reactor was used, with the catalyst bed near the bottom. The catalyst was pre-reduced in a gas flow of 20 vol% H_2/N_2 (25 ml min^{-1}) at 1173 K for 1 h. The thermocouple used to control the reaction temperature was placed at the center of the catalyst bed. Product gases were analyzed by online TCD-gas chromatography. The reaction temperature was fixed at 1073 K so that the stability of the catalyst could be checked for a period of 50 h, during which no significant decrease was observed in the activity. The activity in steam reforming of CH_4 was tested at 1073 K with varying space velocity from 36,000 to 180,000 ml h^{-1} g_{cat}^{-1}. For measurement of the turnover frequency and the effectiveness factor of the catalyst, the reaction temperature was varied from 873 to 973 K, with varying average catalyst particle size from 0.15 to 0.48 mm∅ and varying space velocity of CH_4/H_2O mixed gas from 720,000 to 900,000 ml h^{-1} g_{cat}^{-1}. In both cases, the data were collected at a reaction time of 1 h for each reaction condition.

3. Results

3.1. Effect of temperature of thermal treatment in eggshell-type Ni loading

Some details of the preparation of eggshell-type loaded Ni catalyst were reported previously [33,34]. When Mg–Al(3/1) hydrotalcite prepared by co-precipitation was cal-

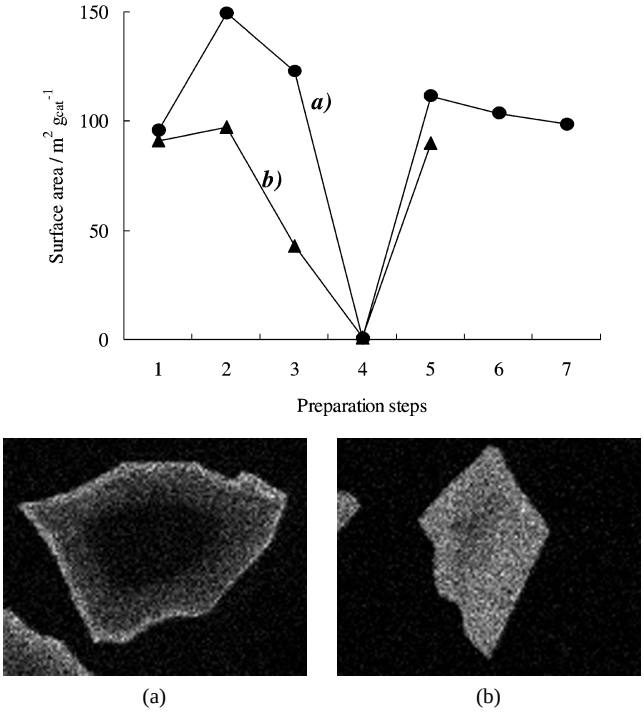

Fig. 1. Surface area of the sample during the preparation of *s-spc*-Ni/MgAl catalyst and SEM image of cross section of the particle after the dipping. Step 1, after the drying of Mg–Al(3/1) hydrotalcite at 378 K; step 2, after the calcination of the sample of step 1; step 3, after the pressing of the sample of step 2, followed by the crushing and the sieving; step 4, after the dipping of the sample of step 3 in Ni^{2+} nitrate aqueous solution, followed by the drying at 378 K; step 5, after the calcination of the sample of step 4 at 1123 K; step 6, after the reduction of the sample of step 5 at 1073 K; step 7, after using the sample of step 6 in steam reforming of CH_4 for 50 h. (a) surface area of the sample calcined at 923 K at step 2 and SEM image after the dipping; (b) surface area of the sample calcined at 1123 K at step 2 and SEM image after the dipping.

cined at 923 K and pressed into the mixed-oxide particles, eggshell-type Ni loading occurred after the particles were dipped in Ni^{2+} nitrate aqueous solution (Fig. 1, SEM image a). On the other hand, when Mg–Al(3/1) hydrotalcite was calcined at 1223 K, Ni penetrated the core of the particle, resulting in a uniform distribution of Ni (Fig. 1, SEM image b). In the XRD results, diffraction lines for periclase Mg(Al)O alone were observed for the Mg–Al(3/1) mixed oxide calcined at 923 K, and lines for $MgAl_2O_4$ spinel appeared together with periclase Mg(Al)O as a main phase in the mixed oxide calcined at 1223 K. After the mixed-oxide particles were dipped in 1.0 M Ni^{2+} nitrate aqueous solution, the Mg–Al hydrotalcite phase was reconstituted for both samples calcined at 923 K and at 1223 K by memory effect [13], though the line intensities were significantly weaker in the latter than in the former. It is assumed that some of the Mg^{2+} sites in the hydrotalcite phases were replaced by Ni^{2+} ions during the reconstitution of hydrotalcite, since both Mg content and MgO line intensity decreased, whereas both Ni content and Mg(Ni)–Al hydrotalcite line intensity increased with increased dipping time [37]. The diffraction lines for MgO were weakened, and those for $MgAl_2O_4$ spinel showed no significant change after the dipping, suggesting that the periclase Mg(Al)O phase alone was converted to Mg(Ni)–Al hydrotalcite. It is concluded that Mg–Al hydrotalcite containing Ni^{2+} at the Mg^{2+} site was reconstituted from periclase Mg(Al)O in both samples treated at 923 and 1223 K, and the reconstitution was more significant in the former than in the latter.

3.2. Surface area during the preparation of s-spc-Ni/MgAl catalyst

BET surface areas of two typical samples taken during the preparation of *s-spc*-Ni/MgAl catalyst are shown in Fig. 1. The numbers on the abscissa show each step during the catalyst preparation and its use in the reaction as follows: step 1, after the drying of Mg–Al(3/1) hydrotalcite at 378 K; step 2, after the calcination of Mg–Al(3/1) hydrotalcite to Mg–Al(3/1) mixed oxide; step 3, after pressing, followed by crushing and sieving; step 4, after dipping of the sample of step 3 in Ni^{2+} nitrate aqueous solution, followed by drying at 378 K; step 5, after calcination of the sample of step 4 at 1123 K; step 6, after reduction of the sample of step 5 at 1073 K; and step 7, after steam reforming of CH_4 at 1073 K for 50 h. Eggshell-type Ni loading appeared when Mg–Al(3/1) hydrotalcite was calcined at 923 K at step 2 (Fig. 1, surface area, a), whereas uniform Ni loading was observed when Mg–Al(3/1) hydrotalcite was calcined at 1123 K at step 2 (Fig. 1, surface area, b). The surface area of Mg–Al(3/1) hydrotalcite was originally ca 100 $m^2\ g_{cat}^{-1}$ after drying at 378 K (step 1) and increased to ca 150 $m^2\ g_{cat}^{-1}$ after calcination at 923 K (Fig. 1a), whereas no significant increase was observed after the calcination at 1123 K (Fig. 1b) (step 2). It was confirmed by TG-DTA that the dehydration of Mg–Al hydrotalcite around 470 K, followed by decomposition to periclase Mg(Al)O Mg–Al(3/1) around 670 K, took place for both samples during the calcination.

Interestingly, surface areas and pore volumes of Mg–Al(3/1) mixed oxides of both samples, a and b, drastically decreased after dipping in 1.0 M Ni^{2+} nitrate aqueous solution at pH 4.7 (step 4). The surface area of the sample calcined at 1123 K was 1.1 $m^2\ g_{cat}^{-1}$, whereas that calcined at 923 K was negligibly small (Table 1). After dipping, XRD observations clearly showed the formation of a mixture of periclase Mg(Al)O and Mg–Al hydrotalcite for both samples, and $MgAl_2O_4$ spinel was also observed for the sample calcined at 1123 K. This drastic decrease in the surface area suggests that during the dipping treatment (step 4) dense surface covering took place on the particles originally possessing porous structure, whereas the presence of $MgAl_2O_4$ moderated this surface covering slightly. After the calcination at 1123 K (step 5), both samples recovered the original surface area of ca 100 $m^2\ g_{cat}^{-1}$. The sample with eggshell-type Ni loading showed no significant decrease in the surface area, not only after the reduction (step 6), but even after the steam reforming of CH_4 at 1073 K for 50 h (step 7).

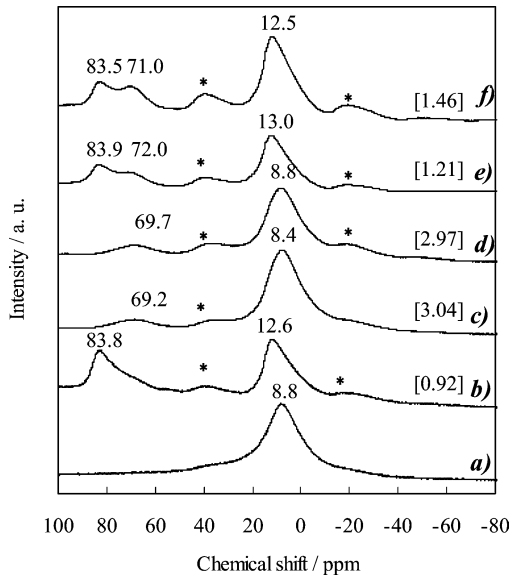

Fig. 2. ^{27}Al NMR spectra of the samples during the preparation of eggshell-type Ni loaded catalyst. (a) Mg–Al(3/1) hydrotalcite; (b) after the calcination of (a) at 1123 K for 5 h (0.83 K min^{-1}); (c) after the dipping of (b) in HNO_3 aqueous solution at pH = 3.0 for 15 min; (d) after the dipping of (b) in 0.1 M Ni^{2+} nitrate aqueous solution at pH = 3.0 for 15 min; (e) after the calcination of (c) at 1123 K for 5 h (1.67 K min^{-1}); (f) after the calcination of (d) at 1123 K for 5 h (1.67 K min^{-1}). *: spinning side band; naked number: chemical shift; number in [ ]: Al_{Oh}/Al_{Td} molar ratio.

3.3. Coordination sphere around Al^{3+} in Mg–Al precursors and Mg–Al(3/1) mixed oxide

Analyses of the MAS ^{27}Al NMR spectra of Mg–Al mixed oxides showed two resonance lines in the regions of 69–84 and 8–13 ppm, which correspond, respectively, to Al^{3+} cations tetrahedrally (Al_{Td}) and octahedrally (Al_{Oh}) coordinated to oxygen [40–42]. Mg–Al hydrotalcite as prepared showed a peak at 8.8 ppm (Fig. 2a). After the calcination at 1123 K (Fig. 2b), the peak shifted to 12.6 ppm, and, moreover, a new peak appeared at 83.8 ppm together with a shoulder at 70 ppm (Fig. 2b). Chemical shifts as a function of the calcination temperature are presented in Fig. 3. The experimental points for Al_{Oh} may be fitted with two lines around 8 and 13 ppm, depending on the calcination temperature below 623 K and above 673 K, respectively. A new chemical shift appeared around 78 ppm at the temperature above 673 K and was then split into two groups, one around 71 ppm and another around 82 ppm above 1073 K. The chemical shift around 8 ppm observed below 623 K coincides with the value observed for Al_{Oh} in Mg–Al hydrotalcite, whereas those around 78 ppm appearing in the range of 623–873 K are probably assigned to Al_{Td} in periclase MgO containing Al^{3+} as solid solutions [42–44]. This indicates that a transition from Al_{Oh} to Al_{Td} took place during the calcination. After the splitting at 1073 K, the chemical shift appearing at 82 ppm is assigned to Al_{Td} bonded to Mg^{2+} (Al_{Td}–O–Mg), whereas that at 71 ppm is assigned to Al_{Td} bonded to Al^{3+} (Al_{Td}–O–Al) [42]. Apparently the transition from Al_{Oh} (8.5 ppm) to Al_{Td} (82 ppm) began to occur at

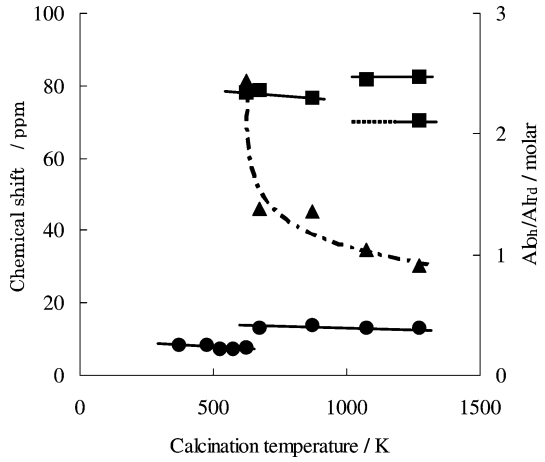

Fig. 3. ^{27}Al NMR analysis of Mg–Al(3/1) mixed oxides prepared from Mg–Al(3/1) hydrotalcite. Effect of the calcination temperature on chemical shift of Al_{Oh} and Al_{Td}, and Al_{Oh}/Al_{Td} molar ratio. ●: Al_{Oh}; ■: Al_{Td}; ▲: Al_{Oh}/Al_{Td} molar ratio.

623 K and continued during the calcination up to 1223 K, since the molar ratio of Al_{Oh}/Al_{Td} continued to decrease with increasing calcination temperature.

According to the results of XRD analyses of the samples, the reflection lines of Mg–Al hydrotalcite were observed below 573 K and were replaced by those of periclase Mg(Al)O at 623 K, almost coinciding with the first phase transition from Al_{Oh} to Al_{Td}. At 623 K the peaks of Mg–Al hydrotalcite were broadened and showed significant tailings toward higher values of 2θ. The reflection lines of periclase Mg(Al)O were observed above 673 K, and those of $MgAl_2O_4$ spinel also appeared above 1073 K, coinciding with the splitting of Al_{Td} to Al_{Td}–O–Mg and Al_{Td}–O–Al. It is assumed that the samples calcined between 673 and 873 K mainly consist of periclase Mg(Al)O, whereas those calcined above 1073 K are mixtures of periclase Mg(Al)O and $MgAl_2O_4$ spinel.

3.4. Pore distribution of Mg–Al(3/1) mixed oxide

Surface area and pore volume of Mg–Al(3/1) hydrotalcite and the mixed oxide after the calcination are shown in Table 1. A large surface area and a large pore volume were observed for both Mg–Al(3/1) hydrotalcite and the mixed oxides prepared by calcination at low temperature, at a small heating rate. Interestingly, after the mixed oxide was dipped in Ni^{2+} nitrate aqueous solution, a drastic decrease was observed not only in the surface area but also in the pore volume.

It was previously mentioned that mild conditions in the calcination of Mg–Al(3/1) hydrotalcite were preferable in the formation of eggshell-type Ni loading [36,37]. Some typical examples of pore distributions for the samples listed in Table 1 are shown in Fig. 4. Mg–Al(3/1) hydrotalcite showed a peak around 2–3 nm together with a wide distribution up to 20 nm in radius (R_p) (Fig. 4A). The lowest limit for pore diameters detectable with the present method is 2 nm, and

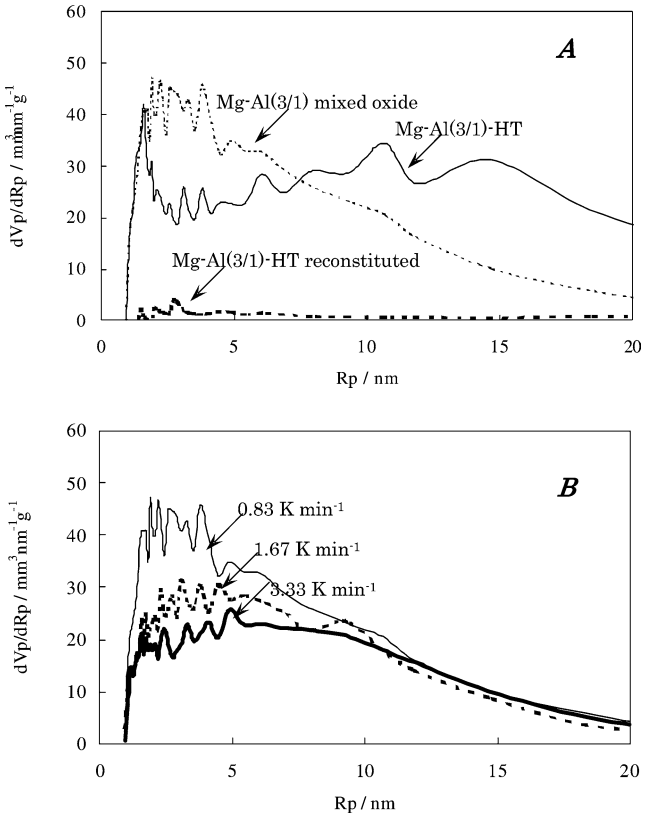

Fig. 4. Pore distributions of Mg–Al(3/1) hydrotalcite and Mg–Al(3/1) mixed oxide. (A) Mg–Al(3/1)-HT: Mg–Al(3/1) hydrotalcite after drying at 378 K; Mg–Al(3/1) mixed oxide: after heating Mg–Al(3/1)-HT at a rate of 0.83 K, followed by calcining at 1123 K for 5 h; Mg–Al(3/1)-HT reconstituted: after dipping Mg–Al(3/1) mixed oxide in 1.0 M Ni^{2+} nitrate aqueous solution. (B) Mg–Al(3/1) hydrotalcite was heated at a rate of 0.83, 1.67, and 3.33 K min^{-1}, followed by calcining at 1123 K for 5 h.

therefore information concerning micropores smaller than 2 nm in diameter could not be obtained. However, SEM images clearly showed a card-like structure probably derived from the layered structures, suggesting that micropores must be retained in the samples after calcination. The former pore sizes are probably related to the layered structure, whereas the latter is due to a "card house" structure consisting of many small plates [37]. We calculated the basal interlayer spacing from the strong symmetric (003) reflection ($2\theta = 13.4°$) of Mg–Al(3/1) hydrotalcite. If the thickness of the brucite-like layer is assumed to be 4.8 Å [45], the interlayer distance corresponds to 2.9 Å. The pore distribution of Mg–Al(3/1) mixed oxide after the calcination at 1123 K (heating rate 0.83 K min^{-1}) converged upon small size and mainly distributed in the area smaller than 5 nm in radius. Several maxima observed in the range up to 5 nm are simply due to the experimental data treatment and have no meaning. Moreover, after the Mg–Al(3/1) mixed oxide was dipped, the pore volume was drastically decreased, as shown by reconstitution of Mg–Al(3/1)-hydrotalcite.

The effect of the heating rate is shown in Fig. 4B. A pore size smaller than 5 nm may again originate from the layered structure, since card-like structures were still observed in the SEM image of mixed oxides heated at a rate of 0.83 K min^{-1}. When the heating rate was increased to 1.67 and further to 3.33 K min^{-1}, pores smaller than 5 nm in radius alone gradually decreased, suggesting that slow heating was preferable for retaining the layered structure originating from hydrotalcite. When the calcination temperature was increased from 823 to 1223 K at a constant heating rate of 1.67 K min^{-1}, the temperature below 923 K was favorable, whereas the temperature above 1023 K was not, for giving a pore distribution smaller than 5 nm. It is concluded that calcination treatment at low temperature or at a small heating rate provides Mg–Al(3/1) mixed oxide with pores smaller than 5 nm in radius, which also play a definitive role in the formation of eggshell-type Ni loading.

3.5. Worm-like structure on s-spc-Ni/MgAl catalyst

SEM observations of the surface of the particles during the preparation of *s-spc*-Ni/MgAl catalysts are shown in Fig. 5. When Mg–Al(3/1) hydrotalcite was calcined at 923 K, plate-like crystals were observed (Fig. 5a) and worm-like structures appeared on the edges of the plates after the dipping for 2 min (Fig. 5b). The numbers of worm-like structures increased with increasing dipping time and finally formed a thick and dense film on the mixed-oxide particles after 20 min (Figs. 5b–5e). After calcination, the structures were significantly shrunken and broken into small pieces (Fig. 5f). Such a transition in the surface morphology explains well the change in the surface area (Fig. 1); the thick and dense film covered the surface of the particle, resulting in a decrease in the surface area. After the dipping treatment, XRD analyses clearly showed the reconstitution of Mg–Al hydrotalcite, and, moreover, SEM-EDS showed eggshell-type Ni incorporation in the particles calcined at 923 K (Fig. 1, SEM image a), whereas uniform Ni was observed in those calcined at 1223 K (Fig. 1, SEM image b). It is believable that the worm-like structures consisted of Mg–Al hydrotalcite, in which some of the Mg^{2+} sites were replaced by Ni^{2+}. The reconstitution of Mg(Ni)–Al hydrotalcite was relatively rapid in the surface layer of mixed-oxide particles calcined at 923 K, resulting in the formation of worm-like structures due to rapid crystal growth. On the other hand, no worm-like structure was observed, but the surface was smooth on the mixed oxide calcined at 1223 K, suggesting that reconstitution of the Mg(Ni)–Al hydrotalcite took place slowly, probably resulting in the formation of thin film [37]. The thin film covered not only the outer surface of the particle but also the inner surface of the pores in the particle, since aqueous Ni^{2+} nitrate solution penetrates into the pores.

3.6. Activity of s-spc-Ni/MgAl catalyst in the reforming of CH_4

The activity of *s-spc*-Ni/MgAl catalyst for the autothermal reforming of CH_4 was briefly reported on in a previous paper [36]. *s-spc*-$Ni_{0.22}/Mg_{2.82}Al$ catalyst was prepared

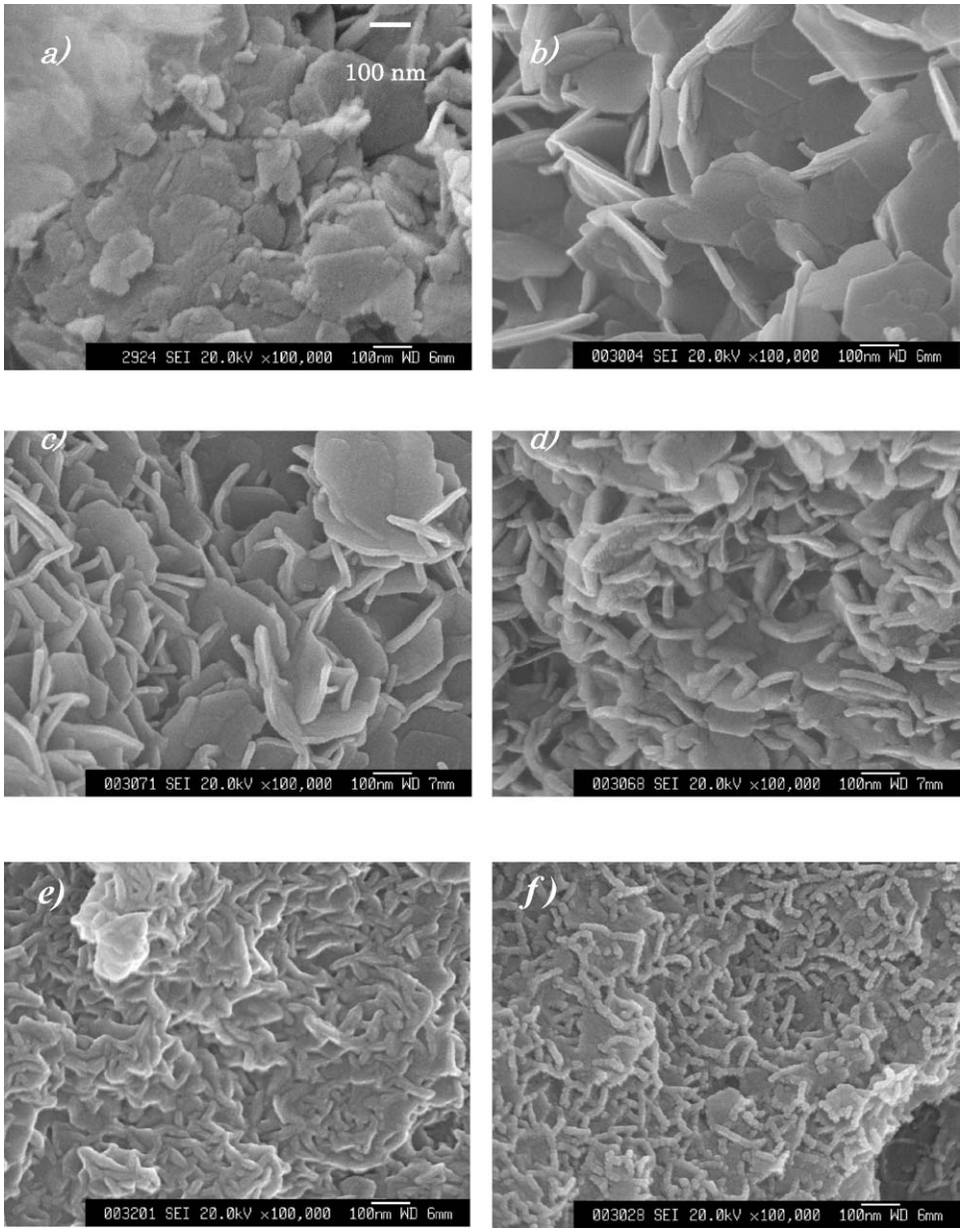

Fig. 5. SEM images of the surface of the samples during the preparation of *s-spc*-Ni/MgAl catalyst. (a) after the drying Mg–Al(3/1) hydrotalcite at 358 K, followed by the calcination at 923 K (1.67 K min^{-1}); (b), (c), (d), and (e) after the dipping of (a) in 0.5 M Ni^{2+} nitrate aqueous solution for 2, 5, 15, and 30 min, respectively, followed by the drying at 378 K; (f) after the re-calcination of (e) at 1223 K (1.67 K min^{-1}).

and tested in steam reforming of CH_4 (Fig. 6), together with *spc*-$Ni_{0.25}/Mg_{2.75}Al$, *imp*-8.2wt%Ni/Mg_3Al-aq, and *imp*-8.2wt%Ni/Mg_3Al-ac. The four catalysts were loaded with almost the same amount of Ni. *s-spc*-$Ni_{0.22}/Mg_{2.82}Al$ showed the highest CH_4 conversion per unit Ni amount at the higher space velocity, that is, at the shorter contact time, followed by *spc*-$Ni_{0.25}/Mg_{2.75}Al$, *imp*-8.2wt%Ni/Mg_3Al-aq, and *imp*-8.2wt%Ni/Mg_3Al-ac. With increasing space velocity, the rate of H_2 formation increased without significant decrease in CH_4 conversion over *s-spc*-$Ni_{0.22}/Mg_{2.82}Al$. Properties and the activities of these catalysts are shown in Table 2 together with those of a larger Ni loading of 16.3 wt%. As mentioned previously, *s-spc*- and *imp*-preparations were carried out by apparently similar procedure, dipping in Ni^{2+} nitrate aqueous solution. Nonetheless, a significant difference was observed in the values of Ni dispersion between *s-spc*-$Ni_{0.22}/Mg_{2.82}Al$ and *imp*-8.2wt%Ni/Mg_3Al-aq and, moreover, between *s-spc*-$Ni_{0.51}/Mg_{2.63}Al$ and *imp*-16.3wt%Ni/Mg_3Al-aq (Table 2). The use of acetone as the solvent for impregnation brought about no memory effect [13,46], resulting in smaller values in both surface area and Ni dispersion for *imp*-8.2wt%Ni/Mg_3Al-ac and *imp*-16.3wt%Ni/Mg_3Al-ac catalysts than for *imp*-8.2wt%Ni/Mg_3Al-aq and *imp*-16.3wt%Ni/Mg_3Al-aq catalysts, respectively. Average sizes of Ni metal particles observed by TEM on *s-spc*-catalysts were close to those observed on the corre-

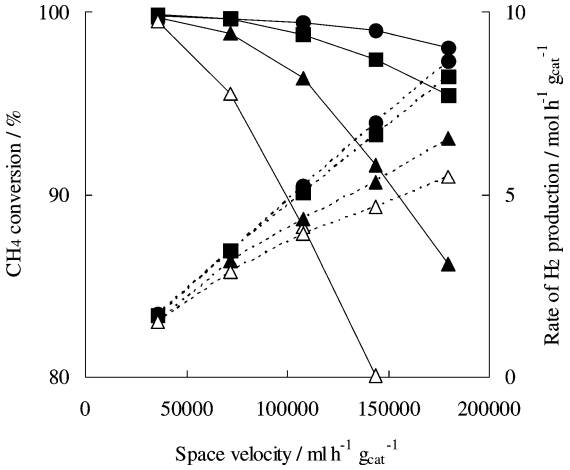

Fig. 6. Activity of *s-spc*-Ni/MgAl catalyst in steam reforming of CH_4. ●: *s-spc*-$Ni_{0.22}/Mg_{2.82}Al$; ■: *spc*-$Ni_{0.25}/Mg_{2.75}Al$; ▲: *imp*-8.2wt%Ni/Mg_3Al-aq; △: *imp*-8.2wt%Ni/Mg_3Al-ac. —: CH_4 conversion (%); - - -: rate of H_2 production (mol h^{-1} g_{cat}^{-1}). Catalyst, 50 mg; CH_4/H_2O = 1/2 (vol).

sponding *spc*-catalysts and far smaller than those on the corresponding *imp*-catalysts. Even though similar values were observed in the Ni dispersion for both *s-spc*-$Ni_{0.22}/Mg_{2.82}Al$ and *spc*-$Ni_{0.25}/Mg_{2.75}Al$, the former showed the higher CH_4 conversion at the higher space velocity. This suggests an important role of the effective enrichment of active Ni species in the surface layer of catalyst particles for the catalytic activity.

The activities of *s-spc*-$Ni_{0.51}/Mg_{2.63}Al$ and *s-spc*-$Ni_{0.22}/Mg_{2.82}Al$ catalysts are shown as both CH_4 conversion and TOF, together with the values of *spc*- and *imp*-Ni/MgAl catalysts (Table 2). Product distribution always followed the thermodynamic equilibrium of the reaction. TOF values were calculated based on the rate of CH_4 consumption at 973 K and at a GHSV of 9.0×10^5 ml h^{-1} g_{cat}^{-1}, and either the amount of surface Ni atom obtained by H_2 adsorption (TOF-s) or the total amount of Ni atom in the catalyst (TOF-t). In both cases, the rate of reaction was measured at CH_4 conversion below 70%. The TOF-s values were approximately the same over each series of *s-spc*-Ni/MgAl, *spc*-Ni/MgAl, and *imp*-Ni/MgAl catalysts with the same Ni loading, suggesting that active Ni species possess the same character regardless of the preparation method. The TOF-s was generally higher than the TOF-t on each catalyst, and, moreover, the TOF-t was higher on *s-spc*-Ni/MgAl than on *spc*-Ni/MgAl catalysts, suggesting that Ni metal was more efficiently concentrated on the surface of *s-spc*-Ni/MgAl than on *spc*-Ni/MgAl.

4. Discussion

4.1. Structure transformation during calcination

It is frequently reported that not only Ni^{2+} [47] but also Al^{3+} [43,48–50] substituted for the Mg^{2+} site in the MgO lattice as solid solutions (i.e., periclase Mg(Al)O containing Ni) when the mixed oxide was prepared by heating of Mg(Ni)–Al hydrotalcite. In the present work, based on XRD data for periclase Mg(Al)O observed for Mg–Al(3/1) mixed oxide, a parameter of the unit cell, *a*, was calculated as 0.41960, 0.42090, and 0.42166 nm after the calcination at 923, 1123, and 1273 K, respectively. When these values are compared with that for pure MgO, 0.42112 nm (JCPDS 45-0948), it is suggested that Al^{3+} is incorporated into MgO as solid solutions at 923 K, whereas this is not the case at 1273 K. After the calcination at 1273 K, periclase Mg(Al)O was transformed to $MgAl_2O_4$ spinel by the release of Al^{3+}. Díez et al. [43] reported that incorporation of Al^{3+} into MgO as solid solutions after the decomposition of Mg–Al hydrotalcite depends essentially on the Mg/Al ratio; however, the effect of the calcination temperature has not been elucidated. As observed in both MAS ^{27}Al NMR spectra and XRD, for the Mg/Al ratio of 3 in the present work, Al^{3+} forms mainly a homogeneous structure into MgO by

Table 2
Property and activity of supported Ni catalysts in steam reforming of CH_4[a]

Catalyst	Surface area (m^2 g_{cat}^{-1})	Ni dispersion (%)	Ni particle size[b] (nm)	CH_4 conversion (%)		TOF-s[e] (s^{-1})	TOF-t[f] (s^{-1})
				[c]	[d]		
s-spc-$Ni_{0.51}/Mg_{2.63}Al$	111.5	14.8	11.2	98.1	70.0	5.8	0.86
s-spc-$Ni_{0.22}/Mg_{2.82}Al$	88.5	12.5	10.6	98.0	45.9	9.0	1.12
spc-$Ni_{0.5}/Mg_{2.5}Al$	178.6	14.7	8.6	96.7	66.4	5.5	0.81
spc-$Ni_{0.25}/Mg_{2.75}Al$	127.3	11.6	9.8	95.5	42.9	9.0	1.05
imp-16.3wt%Ni/Mg_3Al-aq	89.2	9.7	16.1	95.6	60.6	7.7	0.74
imp-16.3wt%Ni/Mg_3Al-ac	72.5	7.0	25.6	82.6	37.9	6.6	0.47
imp-8.2wt%Ni/Mg_3Al-aq	98.7	9.1	–	86.2	36.9	9.9	0.90
imp-8.2wt%Ni/Mg_3Al-ac	33.7	6.1	–	64.6	22.3	8.9	0.54

[a] The catalysts were reduced at 1173 K for 1 h before the reaction. The reaction was carried out at CH_4/H_2O = 1/2.
[b] Measured by TEM.
[c] Obtained at 1073 K and GHSV = 1.8×10^5 ml h^{-1} g_{cat}^{-1}.
[d] Obtained at 973 K and at GHSV = 9.0×10^5 ml h^{-1} g_{cat}^{-1}.
[e] Calculated based on the reaction rate at 973 K and the amount of surface Ni atom measured by H_2 adsorption.
[f] Calculated based on the reaction rate at 973 K and total amount of Ni in the catalyst.

occupying octahedral positions at low calcination temperatures and is converted to tetrahedral coordination by partial formation of the $MgAl_2O_4$ spinel with increasing temperature.

4.2. Mechanism of reconstitution of Mg–Al hydrotalcite

In the MAS ^{27}Al NMR spectra of the samples during the preparation of eggshell-type loaded Ni catalyst, Mg–Al(3/1) hydrotalcite as precipitated showed a peak at 8.8 ppm assigned to Al_{Oh} (Fig. 2a). After the calcination at 1123 K for 5 h (heating rate 0.83 K min^{-1}), two peaks at 12.6 (Al_{Oh}) and 83.8 ppm (Al_{Td}) and a shoulder around 70 ppm (Al_{Td}) were observed, together with spinning side bands (Fig. 2b). This suggests that the hydrotalcite was transformed to periclase Mg(Al)O and $MgAl_2O_4$ spinel, accompanied by a disordering of the structure during calcination. After the oxide was dipped in 0.1 M Ni^{2+} nitrate aqueous solution for 15 min, the peak Al_{Oh} at 12.6 ppm shifted toward the lower value of 8.8 ppm (Fig. 2d), corresponding to the reconstitution of Mg–Al hydrotalcite containing Ni^{2+} in the Mg^{2+} site. At the same time, the peak for Al_{Td}–O–Mg at 83.8 ppm disappeared, whereas that for Al_{Td}–O–Al at 69.7 ppm still remained. An increase in the Al_{Oh}/Al_{Td} ratio after dipping is consistent with the formation of Mg(Ni)–Al hydrotalcite. Appearances of chemical shifts at 12.5, 71.0, and 83.5 ppm after the recalcination of the dipped sample at 1123 K for 5 h (Fig. 2f) clearly indicate the regeneration of both periclase Mg(Al)O containing Ni and $MgAl_2O_4$ spinel. The use of nitric acid instead of Ni^{2+} nitrate resulted in a similar phase transition (Fig. 2 c and e). $MgAl_2O_4$ spinel has been extensively studied by MAS NMR [40–44]. In particular, Shen et al. [41] and MacKenzie et al. [44] studied the thermal decomposition of Mg–Al hydrotalcite by MAS ^{27}Al NMR and XRD. All of these studies observed the migration of cations in the spinel lattice upon heat treatment, usually the migration of Al^{3+} from octahedral to tetrahedral sites, consistent with the present observations. Apparently, a transition of Al^{3+} from octahedral to tetrahedral sites occurs upon calcination at elevated temperature (Fig. 3). According to the XRD results, reflection lines for periclase Mg(Al)O were observed together with weak lines for $MgAl_2O_4$ spinel after the calcination at 1123 K. It is noteworthy that the ^{27}Al NMR peak assigned to Al_{Td}–O–Mg (around 84 ppm) disappeared after dipping and was regenerated after recalcination, whereas that assigned to Al_{Td}–O–Al (around 70 ppm) was not substantially affected during these treatments. This is probably related to the mechanism of reconstitution of Mg–Al hydrotalcite.

The reconstitution of hydrotalcite from Mg–Al mixed oxide may be explained mainly by a dissolution–recrystallization mechanism, contrary to the widely accepted concept of retro-topotactic transformation. The latter mechanism was first proposed on the basis of SEM data: the lamellar structure of natural hydrotalcite was preserved unchanged at heating up to 773 K and after reconstitution in 0.2 M solution of Na_2CO_3 at 353 K for 5 days [51]. Marchi and Apesteguía [46] proposed that the reconstitution of hydrotalcite occurs via a retro-topotactic transformation from the Al^{3+} and divalent cations located in the octahedral sites of the oxide matrix, with the use of Cu–Co–Zn–Al hydrotalcite. Recently it has been reported that both XRD patterns and the surface morphology of the reconstituted hydrotalcite differ substantially from those of the initial samples, suggesting that the reconstitution of hydrotalcite proceeded by a dissolution–recrystallization mechanism [52,53]. When Mg–Al(3/1) hydrotalcite was synthesized, heated at 873 K for 2 h, and dipped in pure water with a natural content of dissolved CO_2 for 24 h at room temperature, the tiny particles stuck to the surface of the initial hydrotalcite plates were entirely converted into spheroidal aggregates of hydrotalcite lamellae [52]. An in situ X-ray diffraction study of the reconstitution of Mg–Al–CO_3^{2-} hydrotalcite-like compounds also assumed the dissolution–recrystallization mechanism [54]. In the present work, dissolution of Mg^{2+} in the solution was clearly observed by ICP analyses, when Mg–Al(3/1) mixed oxide was dipped in a 1.0 M aqueous solution of Ni^{2+} nitrate. Moreover, MAS ^{27}Al NMR spectra showed that the chemical shift of Al_{Td}–O–Mg disappeared, whereas that of Al_{Td}–O–Al remained after the dipping treatment (Fig. 2), also suggesting the dissolution of Mg^{2+}. It was clearly observed by SEM that a worm-like structure started to form on the edge of the plate structure of Mg–Al mixed oxide, grew up independently of the plate structure, and finally formed a crust of hydrotalcite structure possessing a morphology totally different from the original one (Figs. 5a–5e). Periclase Mg(Al)O obtained after the calcination at 673, 873, and 1073 K showed broad reflection lines, and the crystal size was calculated to be 6.9, 7.4, and 8.0 nm, respectively, from the line width of the (200) reflection, indicating that periclase Mg(Al)O was poorly crystallized and exists as aggregates of many small-sized crystals in each plate structure observed in the SEM image (Fig. 5a). This can clearly be seen in Fig. 7a (vide infra). A large number of amorphous structures or at least many defect structures surround these crystallites, from which Mg^{2+} will be dissolved in the solution. Such dissolution may be most frequently observed at the edges of the plate structure, where the defect structures appeared with the largest population. Mg^{2+} in the mixed oxide tends to dissolve in acidic solution at low pH, and as a result the pH of the solution increased, where dissolved Mg^{2+} in the solution tends to be hydrolyzed to form the brucite-like structure. This leads to the formation of hydrotalcite structure in the presence of Al^{3+}, probably because of the tendency toward self-organization as the motive force, as observed in co-precipitation of Mg–Al hydrotalcite. A co-presence of Ni^{2+} in the solution reasonably resulted in the incorporation of Ni^{2+} at the Mg^{2+} site of Mg–Al hydrotalcite. The dissolution of Mg^{2+} and the recrystallization of Mg(Ni)–Al hydro-

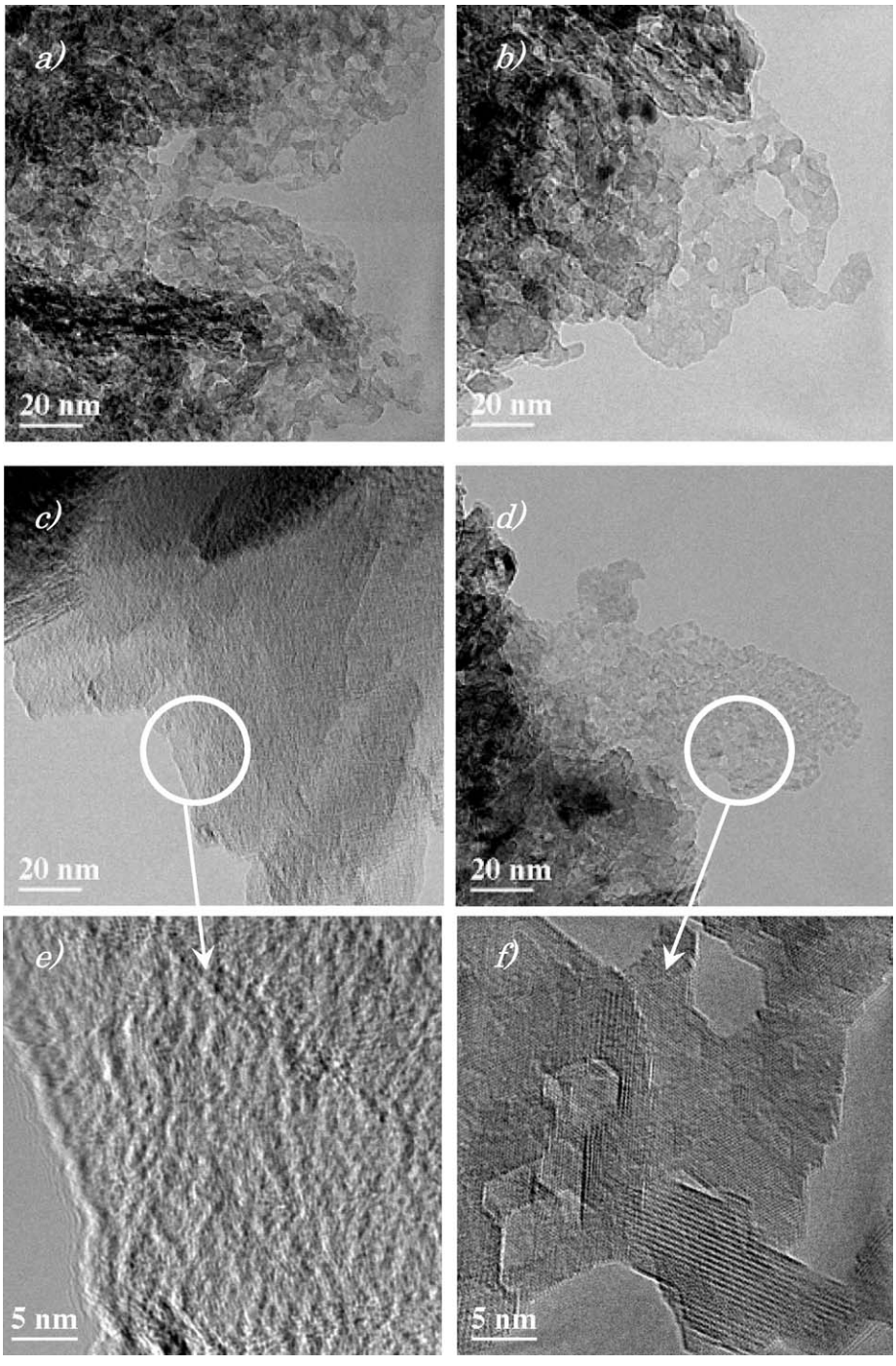

Fig. 7. TEM images of outer edges of Mg–Al(3/1) mixed oxide particles. (a) after the heating of Mg–Al(3/1) hydrotalcite at a rate of 1.67 K min^{-1}, followed by the calcination at 923 K for 5 h; (b) after heating Mg–Al(3/1) hydrotalcite at a rate of 1.67 K min^{-1}, followed by the calcination at 1223 K for 5 h; (c) after the dipping of (a) in 0.5 M Ni^{2+} nitrate aqueous solution for 1 h; (d) after the dipping of (b) in 0.5 M Ni^{2+} nitrate aqueous solution for 1 h; (e) high magnification image of a part in the circle in (c); (f) high magnification image of a part in the circle in (d).

talcite are probably in equilibrium. This mechanism will be valid in the present work but does not exclude the possibility of retro-topotactic transformation as the mechanism of memory effect in general cases. Rocha et al. [55] reported that the reconstitution of Mg–Al hydrotalcite from Mg–Al mixed oxides took place even in the presence of water vapor.

4.3. Mechanism of eggshell-type Ni loading

As described in the previous sections, *s-spc*-Ni/MgAl catalysts were easily prepared by dipping of Mg–Al(3/1) mixed oxide in an aqueous solution of Ni^{2+} nitrate. As far as this technique is concerned, there is principally no significant difference between the *imp*- and *s-spc*- methods, since im-

pregnation in an aqueous solution of Ni^{2+} nitrate was inevitably accompanied by the reconstitution of Mg(Ni)–Al hydrotalcite. The most important point in *s-spc*-preparation is that Ni loading is carefully controlled by the reconstitution of Mg(Ni)–Al hydrotalcite in the surface layer of Mg–Al(3/1) mixed oxide by the memory effect. This means that highly dispersed Ni metal particles, which have already been confirmed to be highly active and stable as *spc*-Ni/MgAl in both steam reforming [9] and autothermal reforming of CH_4 [7], were enriched in the surface layer of the catalyst particle. The catalyst particle is composed of *spc*-Ni/MgAl as the active phase in the surface layer and Mg–Al(3/1) mixed oxide as a core of the particle, resulting in eggshell-type Ni loading.

TEM images of the outer edges of Mg–Al(3/1) mixed-oxide particles obtained by calcination of Mg–Al(3/1) hydrotalcite at 923 and 1223 K are shown in Figs. 7a and 7b, respectively. In both cases, the surface of the particle was covered by aggregates of many small crystallites, in which pore structures were observed, and the crystallite size increased with increasing calcination temperature. The average crystal size was obtained as 7.6 and 13.4 nm after calcination at 923 and 1223 K, respectively, from the line width of the reflection (200) in the XRD. When the mixed-oxide particles were dipped in 1.0 M Ni^{2+} nitrate aqueous solution and dried at 358 K, the surface layer calcined at 923 K was changed to a densely packed structure (Fig. 7c), whereas that at 1223 K still kept its porous structure (Fig. 7d). TEM images of the outer edge of the particle under high magnification (Figs. 7e and 7f) clearly showed that a dense film formed on the particles calcined at 923 K, whereas a crystalline and porous structure was still preserved on the particles calcined at 1223 K. It is concluded that, after the oxide was dipped in Ni^{2+} nitrate aqueous solution, the low calcination temperature bestowed the particles with a thick and dense outer phase consisting of reconstituted Mg(Ni)–Al hydrotalcite, and the high temperature afforded a porous phase. These are consistent with the observations by SEM (Fig. 5) [37]. Rocha et al. [55] studied the reconstitution of Mg–Al hydrotalcite from Mg–Al mixed oxides in the presence of water vapor by XRD and MAS ^{27}Al NMR. It has been found that the reconstitution is complete when the sample is calcined at or below 823 K, whereas only partial reconstitution is observed after calcination at 1273 K.

Eggshell-type Ni loading was realized with Mg–Al(3/1) mixed-oxide particles, on which reconstitution of Mg(Ni)–Al hydrotalcite took place in the surface layer of the particle. Eggshell formation was favored by calcination of the hydrotalcite at low temperature or at low heating rate, where periclase Mg(Al)O was quickly transformed to Mg(Ni)–Al hydrotalcite. When the sample was calcined at high temperature, $MgAl_2O_4$ spinel was formed and retarded this transformation. A pore distribution smaller than 5 nm in radius was preferable for eggshell-type loading, whereas large pores allowed rapid penetration of the bulk of the catalyst particle by Ni. It is concluded that eggshell-type Ni loading was controlled by a balance between the rate of reconstitution of Mg(Ni)–Al hydrotalcite in the surface layer and the rate of penetration of Ni^{2+} nitrate aqueous solution into the bulk. When Mg–Al hydrotalcite was calcined at low temperature, the periclase Mg(Al)O phase was still reactive and quickly converted into Mg(Ni)–Al hydrotalcite, which in turn rapidly formed the dense and thick layer because of pores of a size smaller than 5 nm that were easily filled. Thus Mg(Al)O in the wall of small pores was transformed to Mg(Ni)–Al hydrotalcite, which blocked the small pores and hindered the penetration of the bulk by Ni. It is expected that the thickness and depth of the active Ni layer can be controlled by regulation of the conditions of thermal treatment and dipping.

4.4. Effective surface enrichment of active species in *s-spc*-Ni/MgAl catalyst

It is expected that eggshell-type loaded Ni catalyst shows high activity when the reaction is kinetically limited by intraparticle mass transfer in the steam reforming of CH_4 over the catalyst. In the present work, *spc*-$Ni_{0.5}/Mg_{2.5}Al$ catalyst was used as a model catalyst to elaborate the effectiveness factor, since the surface layer of *s-spc*-Ni/MgAl catalyst is composed of *spc*-Ni/MgAl phase. The effectiveness factor for *spc*-$Ni_{0.5}/Mg_{2.5}Al$ catalyst was calculated based on the reaction rate of the steam reforming of CH_4 at 973 K and at $CH_4/H_2O = 1{:}2$ over the catalysts with varying particle size. At space velocities below 5.4×10^5 $ml\,h^{-1}\,g_{cat}^{-1}$, the rate of reaction significantly depended on the space velocity, indicating that the reaction was completed within a small part of the catalyst bed. With increasing space velocity above 7.2×10^5 $ml\,h^{-1}\,g_{cat}^{-1}$, the reaction rate became nearly constant regardless of the space velocity, indicating that the entire catalyst bed was effective for the reaction. The values of the effectiveness factor were calculated based on the reaction rates at space velocities of 7.2×10^5 and 9.0×10^5 $ml\,h^{-1}\,g_{cat}^{-1}$ by adopting them for the Thiele modulus [56]. As shown in Fig. 8, the effectiveness factor deviated from 1.0 and decreased with increasing particle size of the *spc*-$Ni_{0.5}/Mg_{2.5}Al$ catalyst, clearly indicating that the intraparticle mass transfer limitation exists in the steam reforming of CH_4 over the *spc*-$Ni_{0.5}/Mg_{2.5}Al$ catalyst. The particle size of the *s-spc*-Ni/MgAl catalyst used in the present work was the largest one, 0.36–0.60 mm∅, and the surface of the catalyst particle is inevitably composed of *spc*-Ni/MgAl. It is concluded that the reforming reaction over *s-spc*-Ni/MgAl catalyst proceeded in micro- and mesoporous spaces located in surface layer of the catalyst particles, where highly dispersed Ni metal particles are concentrated by *s-spc*-preparation and effectively catalyze the reaction.

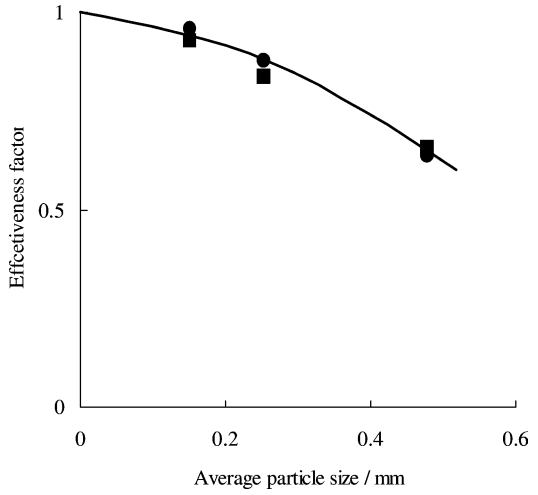

Fig. 8. Effectiveness factor of *spc*-$Ni_{0.5}/Mg_{2.5}Al$ catalyst in steam reforming of CH_4. Reaction temperature, 973 K; Average particle size of the catalyst, 0.15–0.48 mm∅. GHSV: ■, 7.2×10^5 $ml\,h^{-1}\,g_{cat}^{-1}$; ●, 9.0×10^5 $ml\,h^{-1}\,g_{cat}^{-1}$.

5. Conclusion

The mechanism of eggshell-type Ni loading on Mg–Al mixed oxide was discussed in relation to the surface and crystal structure of the mixed oxide as investigated by XRD, MAS-NMR, TG-DTA, SEM, TEM, ICP, and the N_2 and H_2 adsorption methods. We prepared particles of Mg–Al mixed oxide by calcining Mg–Al hydrotalcite and dipping it in an aqueous solution of Ni^{2+} nitrate. During this treatment, reconstitution of Mg–Al hydrotalcite took place by a "memory effect" on the surface layer of the mixed oxide, and simultaneously Ni^{2+} was incorporated by replacement of the Mg^{2+} site. The precursors obtained by the reconstitution were recalcined and reduced to form catalysts loaded by Ni in eggshell-type. The formation of eggshell-type Ni loading was substantially affected by the calcination conditions of Mg–Al(3/1) hydrotalcite; a low heating rate and a low calcination temperature were preferable. When Mg–Al(3/1) mixed oxide was prepared by calcination at a low heating rate or at a low temperature, periclase Mg(Al)O was mainly formed, on which reconstitution of Mg(Ni)–Al hydrotalcite took place rapidly to form a dense and thick layer that covered the surface of the mixed-oxide particles, finally resulting in eggshell-type Ni loading. When $MgAl_2O_4$ spinel was formed by calcination at high temperature, the surface reconstitution of Mg(Ni)–Al hydrotalcite was slow and an aqueous solution of Ni^{2+} nitrate rapidly penetrated the particle, resulting in a uniform distribution of Ni in the catalyst particles. The eggshell-type loaded Ni catalyst showed higher activity per unit Ni amount than the other catalysts in steam reforming of CH_4 into synthesis gas. It was confirmed that the reaction was controlled by intraparticle diffusion by measurement of the effectiveness factor of the catalyst, and the high activity was mainly due to the surface enrichment of active Ni species.

Acknowledgments

The authors sincerely thank the Hiroshima Industrial Technology Organization and the New Energy and Industrial Technology Development Organization for financial support.

References

[1] M.A. Pena, J.P. Gomez, J.L.G. Fierro, Appl. Catal. A 144 (1996) 77.
[2] J.N. Armor, Appl. Catal. A 176 (1999) 159.
[3] J.R. Rostrup-Nielsen, Catal. Today 71 (2002) 243.
[4] T. Hayakawa, H. Harihara, A.G. Andersen, A.P.E. York, K. Suzuki, H. Yasuda, K. Takehira, Angew. Chem., Int. Ed. Engl. 35 (1996) 192.
[5] K. Takehira, T. Shishido, M. Kondo, J. Catal. 207 (2002) 307.
[6] T. Shishido, M. Sukenobu, H. Morioka, M. Kondo, Y. Wang, K. Takaki, K. Takehira, Appl. Catal. A 223 (2002) 35.
[7] K. Takehira, T. Shishido, P. Wang, T. Kosaka, K. Takaki, J. Catal. 221 (2004) 43.
[8] T. Shishido, P. Wang, T. Kosaka, K. Takehira, Chem. Lett. (2002) 752.
[9] K. Takehira, T. Shishido, P. Wang, T. Kosaka, K. Takaki, Phys. Chem. Chem. Phys. 5 (2003) 3801.
[10] T. Shishido, M. Sukenobu, H. Morioka, R. Furukawa, H. Shirahase, K. Takehira, Catal. Lett. 73 (2001) 21.
[11] A.I. Tsyganok, K. Suzuki, S. Hamakawa, K. Takehira, T. Hayakawa, Catal. Lett. 77 (2001) 75.
[12] A.I. Tsyganok, T. Tsunoda, S. Hamakawa, K. Suzuki, K. Takehira, T. Hayakawa, J. Catal. 213 (2003) 191.
[13] F. Cavani, F. Trifiro, A. Vaccari, Catal. Today 11 (1991) 173.
[14] O. Clause, M. Gazzano, F. Trifiro, A. Vaccari, L. Zatorski, Appl. Catal. 73 (1991) 217.
[15] E.C. Kruissink, L.L. Van Reijen, J.R.H. Ross, J. Chem. Soc. Faraday Trans. 1 77 (1991) 649.
[16] G. Fornasari, M. Gazzano, D. Matteuzzi, F. Trifiro, A. Vaccari, Appl. Clay Sci. 10 (1995) 69.
[17] F. Basile, L. Basini, G. Fornasari, M. Gazzano, F. Trifiro, A. Vaccari, J. Chem. Soc. Chem. Commun. (1996) 2435.
[18] F. Basile, L. Basini, M. D'Amore, G. Fornasari, A. Guarinoni, D. Matteuzzi, G. Del Piero, F. Trifiro, A. Vaccari, J. Catal. 173 (1998) 247.
[19] F. Basile, G. Fornasari, E. Poluzzi, A. Vaccari, Appl. Clay Sci. 13 (1998) 329.
[20] F. Basile, G. Fornasari, M. Gazzano, A. Vaccari, Appl. Clay Sci. 16 (2000) 185.
[21] F. Basile, G. Fornasari, F. Trifiro, A. Vaccari, Catal. Today 64 (2001) 21.
[22] F. Basile, G. Fornasari, M. Gazzano, A. Kiennemann, A. Vaccari, J. Catal. 217 (2003) 245.
[23] A. Bhattacharyya, W.-D. Chang, M.S. Kleefisch, M.S. Udovich, U.S. Patent 5,399,537 (1995).
[24] A. Bhattacharyya, W.-D. Chang, M.S. Kleefisch, M.S. Udovich, U.S. Patent 5,591,238 (1997).
[25] A. Bhattacharyya, W.-D. Chang, M.S. Kleefisch, M.S. Udovich, U.S. Patent 5,653,774 (1997).
[26] A. Bhattacharyya, V.W. Chang, D.J. Schumaccher, Appl. Clay Sci. 13 (1998) 317.
[27] Z. Hou, T. Yashima, Appl. Catal. A 261 (2004) 205.
[28] K. Schulze, W. Makowski, R. Chyzy, R. Dziembaj, G. Geismar, Appl. Clay Sci. 18 (2001) 59.
[29] E. Ruckenstein, H.Y. Wang, Appl. Catal. A 198 (2000) 33.
[30] I.J. Alcaraz, B.J. Arena, R. Gillispie, J.S. Holmgrene, Proceedings 15th Meeting of the North Ammerican Catalysis Society, Chicago, 1997, p. 114.
[31] Ph. Courty, Ch. Marcilly, in: G. Poncelet, P. Grange, P.A. Jacobs (Eds.), Preparation of Catalysts III, Elsevier, Amsterdam, 1983, p. 485.

[32] D. Tichit, M. Naciri Bennani, F. Figueras, R. Tessier, J. Kervennal, Appl. Clay Sci. 13 (1998) 401.
[33] K.K. Rao, M. Gravelle, J.S. Valente, F. Figueras, J. Catal. 173 (1998) 115.
[34] F. Prinetto, D. Tichit, R. Tessier, B. Coq, Catal. Today 55 (2000) 103.
[35] J.C.A.A. Roelofs, A.J. van Dillen, K.P. de Jong, Catal. Today 60 (2000) 297.
[36] K. Takehira, T. Shishido, D. Shouro, K. Murakami, M. Honda, T. Kosaka, T. Kawabata, K. Takaki, Catal. Commun. 5 (2004) 209.
[37] K. Takehira, T. Shishido, D. Shouro, K. Murakami, M. Honda, T. Kawabata, K. Takaki, Appl. Catal. A, in press.
[38] M. Miyata, A. Okada, Clays Clay Miner. 25 (1977) 14.
[39] D. Dollimore, G.R. Heal, J. Appl. Chem. 14 (1964) 109.
[40] A.L. McKenzie, C.T. Fishel, R.J. Davis, J. Catal. 138 (1992) 295.
[41] J. Shen, M. Tu, C. Hu, J. Solid State Chem. 137 (1998) 295.
[42] M.A. Armendía, V. Borau, C. Jiménez, J.M. Luque, J.M. Marinas, J.R. Ruiz, F.J. Urbano, Appl. Catal. A 216 (2001) 257.
[43] V.K. Díez, C.R. Apesteguía, J.I. Di Cosimo, J. Catal. 215 (2003) 220.
[44] K.J.D. MacKenzie, R.H. Meinhold, B.L. Sherriff, Z. Xu, J. Mater. Chem. 3 (1993) 1263.
[45] M.A. Drezdon, Inorg. Chem. 37 (1988) 4628.
[46] A.J. Marchi, C.R. Apesteguía, Appl. Clay Sci. 13 (1998) 35.
[47] A. Parmaliana, F. Arena, F. Frusteri, A. Giordano, J. Chem. Soc. Faraday Trans. 1 86 (1990) 2663.
[48] D.C. Puxley, I.J. Kitchener, C. Komodromos, N.D. Parkins, Stud. Surf. Sci. Catal. 16 (1983) 237.
[49] J.R.H. Ross, Catalysis, Specialist Periodical Reports, vol. 7, Royal Society of Chemistry, London, 1985, p. 1.
[50] B. Rebours, J.B. d'Espionose de la Caillerie, O. Clause, J. Am. Chem. Soc. 116 (1994) 1707.
[51] T. Sato, H. Fujita, T. Endo, M. Shimada, A. Tsunashima, React. Solids 5 (1988) 219.
[52] T. Stanimirova, G. Kirov, E. Dinolava, J. Mater. Sci. Lett. 20 (2001) 453.
[53] T. Stanimirova, G. Kirov, Appl. Clay Sci. 22 (2003) 295.
[54] F. Millange, R.I. Walton, D. O'hare, J. Mater. Sci. 10 (2000) 1713.
[55] J. Rocha, M. del Arco, V. Rives, M.A. Ulibarri, J. Mater. Chem. 9 (1999) 2499.
[56] O. Levenspiel, Chemical Reaction Engineering, second ed., Wiley, New York, 1972, p. 460.